LETTER

Realization of flexible AlGaN/GaN HEMT by laser liftoff

Applied Physics Express 15, 071011 (2022)
https://doi.org/10.35848/1882-0786/ac7847

LETTER

Realization of flexible AlGaN/GaN HEMT by laser liftoff

Md Didarul Alam*, Kamal Hussain, Shahab Mollah, Grigory Simin, Asif Khan, and MVS Chandrashekhar

Department of Electrical Engineering, University of South Carolina, Columbia, SC 29208, United States of America

*E-mail: ma57@email.sc.edu

Received May 24, 2022; revised June 7, 2022; accepted June 12, 2022; published online June 29, 2022

We demonstrate fully fabricated AlGaN/GaN high electron mobility transistors (HEMTs) transferred from sapphire to copper tape on flexible polyethylene terephthalate using 193 nm excimer laser liftoff (LLO). The heterojunction is structurally intact after LLO, leading to preserved electron mobility $\mu_n \sim 1630\ cm^2\ V^{-1}\ s^{-1}$ and carrier concentration $n_s \sim 10^{13}\ cm^{-2}$. The maximum drain saturation current decreased by ~18% after transfer, which is a lower reduction than other reported transfer methods. The drain current of this flexible HEMT increased monotonically under tensile stress applied using a convex-shaped plate, while the threshold voltage shifted more negative in quantitative agreement with the expected piezoelectric charge for an intact heterojunction. © 2022 The Japan Society of Applied Physics

Owing to the advantages of high electron mobility, high sheet carrier concentration, high electric breakdown field, and high-temperature stability, flexible electronic/optoelectronic devices based on wide bandgap materials have shown a rapid trend of development due to demand in a wide range of commercial and military applications. AlGaN/GaN high electron mobility transistors (HEMTs) are typically fabricated on rigid substrates such as Si, sapphire, or SiC which cannot meet the requirements for application in deformed and nonplanar environments.[1–6] Several groups have reported transfer of AlGaN/GaN HEMT structures from rigid substrates to various flexible substrates with different transfer technologies as listed in Table I. Demonstration of flexible AlGaN/GaN HEMT on 3 M adhesive tapes with different thermal conductivities by the mechanical lapping and etching method to remove the Si substrate were reported.[7–9] Wet chemical etching was also used to transfer GaN HEMT arrays onto copper tape,[10] Kapton tape,[11] and polyethylene terephthalate (PET).[12] Glavin et al. mechanically transferred HEMTs to a 3 M adhesive substrate using h-BN as the sacrificial layer.[13] Recently, conductivity-selective electrochemical etching to realize flexible HEMTs by removing growth substrate was reported.[14,15]

There are some disadvantageous associated with these transfer technologies. The most widely used approaches to transfer GaN electronics from Si to a flexible substrate are by removing it through mechanical grinding followed by xenon difluoride (XeF_2) etching and wet etching result in the degraded backside because of the harsh acidic environment, as well as the strong surface tension of water that is unavoidable at these dimensions.[12] These techniques are also complicated and time-consuming. Moreover, epitaxial growth of GaN on Si requires additional growth steps due to the significant lattice and coefficient of thermal expansion mismatch[16] and is typically of lower quality compared to the high-temperature growth on sapphire, SiC or bulk GaN/AlN substrates which are difficult to grind and wet-chemically etch.[17,18] Therefore, the reported transfer techniques from Si substrate to arbitrary flexible substrates are not applicable to fabricating ultra-wide bandgap (UWBG) III-nitride flexible devices. Growth of uniform large-area h-BN between AlGaN/GaN heterostructure and substate for mechanical transfer is difficult and it is hard to completely peel off large-area AlGaN/GaN membrane.[12] Electrochemical etching by introducing a highly doped GaN sacrificial layer damages the effective area and integrity of the released GaN layer.[14] Moreover, these reported flexible GaN-channel HEMTs showed significantly reduced maximum drain currents after transfer (Table I). Therefore, it is important to develop a method that offers a more efficient and reliable large-area transfer of AlGaN/GaN devices to flexible substrates while minimizing the peak current reduction.

In this paper, we demonstrate the transfer of AlGaN/GaN HEMTs from sapphire to flexible copper tape by an excimer laser liftoff (LLO) technique. The crystalline quality of the AlGaN/GaN heterostructure is preserved during transfer. The fabricated devices exhibit maximum drain saturation current density ($I_{DS,\ max}$) of 422 and 347 mA mm^{-1} before and after transfer, respectively. Even without AlN heat spreaders,[19–21] this ~18% degradation after transfer is lower than that of other reported transfer techniques (Table I). In this work, the effect of external stress on the active current modulation to prove the concept of polarization engineering is also investigated. Our scalable LLO approach, in principle, should also be applicable to UWBG AlGaN channel flexible HEMTs for electronics needing high-temperature, high-frequency, and high-power operation. We also present a detailed approach to evaluate the remaining average GaN channel epilayer thickness after the LLO process and the post-processing which is required to remove a portion of the damaged interfacial material. This evaluation of the remaining thickness is important for thin channel devices and was not addressed in previous transfer demonstrations.

The AlGaN/GaN HEMT structure used in this study was grown on a double-side polished (DSP) sapphire substrate by metal-organic chemical vapor deposition. The epitaxial wafer consists of a 30 nm GaN nucleation layer, a 1.8 μm unintentionally doped GaN buffer and channel layer, a 1 nm AlN spacer, and a 17 nm $Al_{0.24}Ga_{0.76}N$ barrier layer. Device processing was started with mesa isolation using Cl_2-based inductively coupled plasma reactive-ion etching. Ti/Al/Ti/Au (15/70/30/50 nm) metal stack was deposited by electron beam (e-beam) evaporation as source/drain electrodes followed by rapid thermal annealing at 850 °C for 30 s in N_2 environment. The ohmic contact resistance measured by the transmission line model (TLM) was found to be 0.59 Ω mm. Ni/Au (50/150 nm) were deposited as the gate electrodes by e-beam evaporation. Gate length, gate width, and source-to-drain spacing were 2 μm, 50 μm, and 6 μm, respectively.

The LLO technique was used to transfer the fabricated AlGaN/GaN HEMTs from DSP sapphire to flexible copper

Table I. Summary of the comparative performance of previously reported flexible AlGaN/GaN HEMTs realized by different transfer methods.

References	Transfer method	$I_{DS,max}$ (rigid substrate) mA/mm	$I_{DS,max}$ (flexible substrate) mA/mm	% of decrease in $I_{DS,\,max}$
This work	LLO	422	347	17.8
Defrance et al.[7]	Lapping and XeF_2 etching	930	450	51.6
Lesecq et al.[8]	Lapping and XeF_2 etching	1200 (TLM)	690 (TLM)	42.5
Mhedhbi et al.[9]	Lapping and XeF_2 etching	Not mentioned	275	—
Zhu et al.[10]	Chemical wet etching	457	290	36.5
Hsu et al.[11]	Chemical wet etching	753	290	61.5
Zhang et al.[12]	Chemical wet etching	226	110	51.3
Glavin et al.[13]	Mechanical transfer	Not mentioned	Not mentioned	—
Chen et al.[14]	Electrochemical etching	Not mentioned	106	—
Chang et al.[15]	Electrochemical etching	753	290	61.5

tape (see Fig. 1). After the devices were fabricated, the epitaxial side of the sample was bonded to a temporary carrier substrate (UV tape), and a 193 nm ArF excimer laser with a fluence of 800 mJ cm^{-2} was used to remove the DSP sapphire. The exposed GaN surface was etched with 1:1 dilute HCl to remove the damaged layer and bonded to a copper tape with adhesive on both sides. The other side of the copper tape was bonded to a flexible PET substrate for ease of handling. Finally, the UV tape was removed after exposing it in a UV curing chamber. Our transfer process involves no harsh chemicals which result in a low-damage transfer keeping the epilayer intact. The schematic of the transfer process by LLO is shown in Figs. 1(a)–1(d). The optical images of the HEMTs before and after transfer are shown in Figs. 1(e)–1(h). To assess the quality of the epitaxial layer before and after transfer, high-resolution X-ray diffractometry (HRXRD) was done using a triple-axis diffractometer at a wavelength, $\lambda = 0.154$ nm and cathodoluminescence (CL) spectra were measured using a scanning electron microscope equipped with a parabolic mirror spectrometer. The output and transfer characteristics of the HEMT before and after transfer were measured using a parameter analyzer, while the capacitance–voltage (C–V) measurement was done using an LCR Meter.

Figure 2(a) shows the (002) ω–2θ coupled scan of the $Al_{0.24}Ga_{0.76}N$/GaN HEMT before and after transfer. After transfer, the relative biaxial strain of the barrier layer and the epitaxial registry are preserved. The FWHM of GaN along the (002) plane before and after transfer are 302 and 345 arcsecs, respectively (see supplementary data) depicting a low-damage transfer process and conservation of crystal quality. This is also supported by the on-mesa and off-mesa counts from CL spectra taken at different acceleration voltages as shown in Fig. 2(b) (also see supplementary data).

The sheet carrier concentration (n_s) before and after transfer was measured from frequency-dependent C–V characteristics (Fig. 3) using the following equation:[22]

$$qn_s = \int_{V_{min}}^{0} C_{G1}(V_{GS})dV_{GS} \quad (1)$$

where q is the electron charge, V_{min} is applied voltage lower than the threshold voltage (V_{th}), C_{G1} is the gate capacitance per unit area , and V_{GS} is the gate–source voltage. The calculated sheet carrier densities n_s are $\sim 9.8 \times 10^{12}$ cm^{-2} before and after transfer, showing that the 2DEG is intact through the LLO process. No dispersion is observed in the frequency-dependent C–V suggesting no additional possible traps and defects are introduced within the structure after transfer (see supplementary data).

Figure 4(a) presents the output characteristics of the AlGaN/GaN HEMTs on sapphire and copper tape. The $I_{DS,\,max}$ decreased from 422 mA mm^{-1} for HEMTs on sapphire to 347 mA mm^{-1} for HEMTs on copper tape. $I_{DS,\,max}$ decreased by ~18%, which is the lowest reported decrease for depletion mode HEMTs transferred onto similar flexible substrates without heat spreaders. Drain current density (I_{DS}) decreased by 5.7% when V_{DS}. changed from 5 to 10 V at $V_{GS} = 1$ V on sapphire, while it decreased by 17.6% on copper tape due to thermal droop. This current degradation is attributed to the large difference in thermal conductivities between sapphire ($k \sim 34.6$ W mK^{-1}) and the adhesive on copper tape (~0.5 W mK^{-1}), which is not efficient in dissipating generated heat. This can be mitigated by using integrated epitaxial AlN heat spreaders.[19]

Figure 4(b) shows the comparison of transfer characteristics and transconductances (g_m) of HEMTs on sapphire and copper tape at $V_{DS} = 8$ V. The maximum transconductances ($g_{m,\,max}$) for devices on sapphire and copper tape are 0.11 and 0.08 S mm^{-1}, respectively. After transfer, V_{th} shifted negatively from −3.5 to −3.8 V. From the TLM measurements before and after transfer, the contact resistances (R_C) are found to be 0.59 and 0.64 Ω mm, respectively while the sheet resistance (R_{sh}) increased slightly from 380 to 390 Ω sq^{-1}. (see supplementary data). Using the values of R_{sh} and n_s, the carrier mobility μ_n is:

$$\mu_n = \frac{1}{qR_{sh}n_s} \quad (2)$$

The μ_n in the 2D channel is found to be ~1670 cm^2 V^{-1} s^{-1} for the devices on sapphire while it decreased marginally to ~1630 cm^2 V^{-1} s^{-1} for devices on copper tape, underscoring the integrity of the heterojunction through transfer.

To analyze the piezoelectric effect on the flexible AlGaN/GaN HEMT under external tensile stress in the gate width direction, a convex-shaped aluminum (Al) plate with different radii of curvatures $R = 0.3$, 0.5, and 1 cm was used to induce the bending. The I–V characteristics of the HEMTs under flat and bent conditions are shown in Fig. 5. When the flexible HEMT structures are bent downward [Fig. 5(a) inset], tensile stress induces additional piezoelectric polarizations in AlGaN, therefore, increasing both polarization

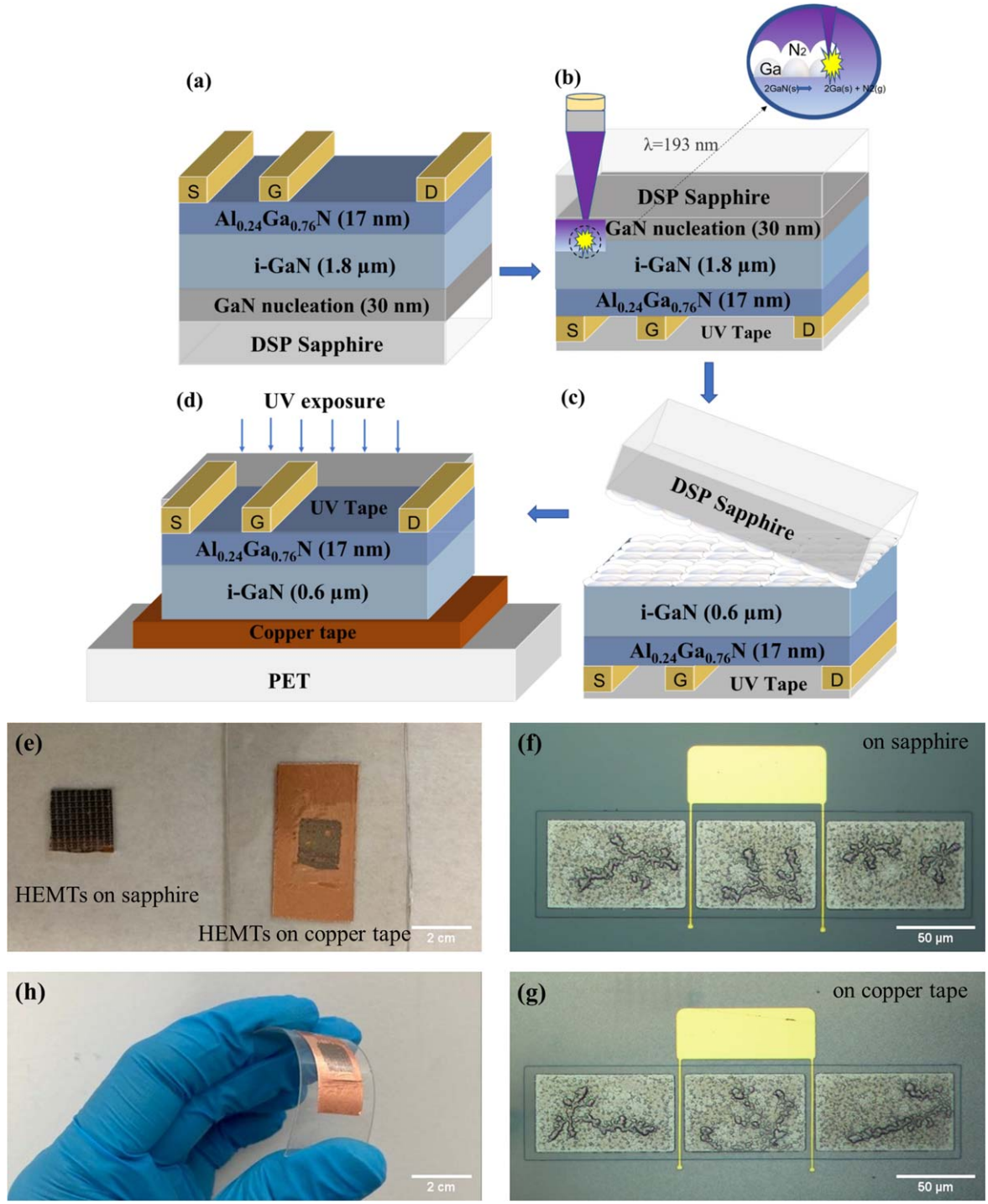

Fig. 1. (Color online) Schematic process flow for the realization of flexible AlGaN/GaN HEMT by LLO. (a) Device structure of the as-fabricated HEMT on DSP sapphire. (b) Metal contact side of the devices was bonded to a temporary carrier substrate (UV tape) and DSP sapphire side was exposed to laser acting on the GaN/DSP sapphire interface dissociating GaN into Ga(s) and N_2(g). (c) Sapphire was removed. (d) Exposed GaN surface was cleaned and bonded to a double-sided copper tape carried by PET. The UV tape was removed after UV exposure. Optical microscope images of the HEMT (e) before and after transfer. Devices on (f) sapphire, and (g) copper tape. (h) Flexible GaN HEMTs under stress conditions.

induced charge Q_{AlGaN} and n_s, leading to the measured increase in I_{DS} [Fig. 5(a)] and more negative V_{th} [Fig. 5(b)]. I_{DS} at $V_{GS} = -3$ V and $V_{DS} = 10$ V increased from 43 to 52 mA mm^{-1}, while V_{th} shifted more negative from -3.8 to -4.1 V as the device goes from flat to $R = 0.3$ cm condition.

This negative V_{th} shift indicates that more carriers are induced by bending, in line with increased I_{DS} observed [Fig. 5(a)]. This is due to the external tensile stress-inducing piezoelectric charge at the AlGaN/GaN junction, modulating 2DEG carrier concentration n_s.[23)]

$$n_s = Q_{AlGaN} - \frac{\varepsilon_{AlGaN}\,\varepsilon_0}{q^2 d_{AlGaN}}\left(q(\varphi_{bi} - V_{GS}) + E_f - \Delta E_C\right) \quad (3)$$

where Q_{AlGaN}, ε_{AlGaN}, and d_{AlGaN} are the polarization induced charge, relative dielectric constant, and thickness of the AlGaN barrier, respectively. φ_{bi} is the surface barrier height, $E_f = 0.15$ eV is the Fermi level with respect to the conduction band edge of GaN at the AlGaN/GaN interface, and $\Delta E_C = 0.45$ eV is the AlGaN/GaN interface conduction band offset. $q\varphi_{bi} = 2.5$ eV, is experimentally obtained from

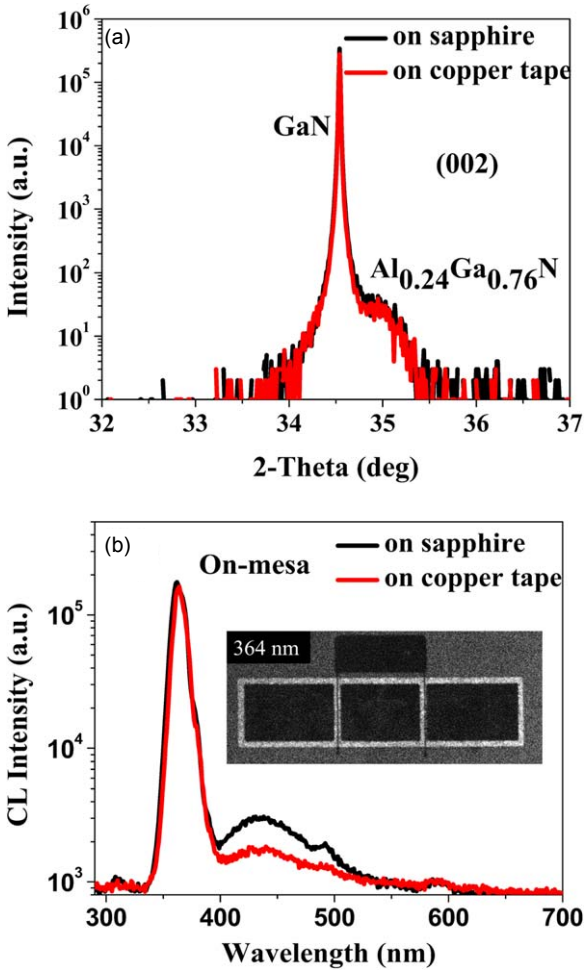

Fig. 2. (Color online) (a) HRXRD (002) ω–2θ coupled scan illustrates the preservation of the epitaxial registry of the AlGaN/GaN junction after transfer. (b) On-mesa CL spectra at the acceleration voltage of 20 kV. Inset shows CL image of the flexible AlGaN/GaN HEMT taken at GaN band edge wavelength.

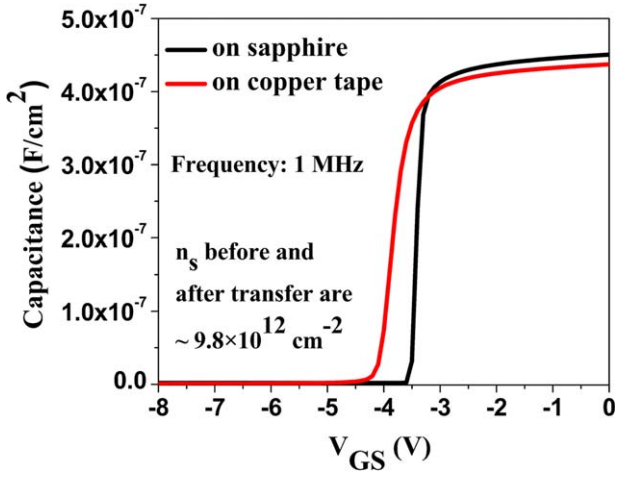

Fig. 3. (Color online) Frequency-dependent C–V profiles on sapphire, and copper tape carried out at 1 MHz. Sheet carrier concentrations n_s before and after transfer are $\sim 9.8 \times 10^{12}$ cm^{-2}.

the x-intercept of the $1/C^2$ versus V_{GS} characteristic of the LLO transferred device (see supplementary data). The first term on the right-hand side of Eq. (3) shows the free carriers induced by polarization, while the second term describes the depletion of carriers from the surface barrier at applied V_{GS}. Under flat condition, C–V gives $n_s = \sim 10^{13}$ cm^{-2} at $V_{GS} = 0$ (Fig. 3) while at $V_{GS} = V_{th}$, the channel is fully depleted ($n_s = 0$) giving two Eqs. (4a) and (4b) from Eq. (3). When these two equations are solved simultaneously, it gives $d_{AlGaN} = 17$ nm which is in excellent agreement with the nominal thickness of 20 nm as calculated from the epilayer growth rate, and correctly predicts the $C_{GS}(V_{GS} = 0) = 0.44\ \mu F\ \text{cm}^{-2}$ as measured. For subsequent measurements under tensile stress, this d_{AlGaN} value was used in Eq. (3) with a fully depleted channel $n_s = 0$ at $V_{GS} = V_{th}$, so that the measured V_{th} provides a direct extraction of Q_{AlGaN} for each R. Given that the spontaneous contribution to Q_{AlGaN} is fixed,[24] any change to Q_{AlGaN} from tensile strain is due to piezoelectric charge.

Considering uniaxial deformation with no directional preference as described by Defrance et al,[7] the polarization charge under flat condition $Q_{AlGaN}(1/R = 0)$ is increased by ΔQ_{AlGaN} and given by:

$$Q_{AlGaN}(1/R) = Q_{AlGaN}(0) + \Delta Q_{AlGaN}(1/R) \tag{4a}$$

$$\begin{aligned} q\Delta Q_{AlGaN} &= \frac{\sigma_{tensile}\left(e_{31} - e_{33}\dfrac{C_{13}}{C_{33}}\right)}{(C_{11} + C_{12}) - 2\dfrac{C_{13}^2}{C_{33}}} \\ &= \frac{\sigma_{tensile}\left(e_{31} - e_{33}\dfrac{C_{13}}{C_{33}}\right)}{Y_{AlGaN}} \\ &= \frac{1}{R}\frac{d_{GaN}^2}{6(1-\upsilon_s)d_{AlGaN}}\frac{Y_{GaN}}{Y_{AlGaN}}\left(e_{31} - e_{33}\frac{C_{13}}{C_{33}}\right) \end{aligned} \tag{4b}$$

where $\sigma_{tensile}$, e, and C are the tensile stress, piezoelectric constants, and elastic constants of AlGaN, respectively, with the Stoney equation giving $\sigma_{tensile}$[25] as a function of the radius of curvature

$$\sigma_{tensile} = \frac{Y_{GaN} d_{GaN}^2}{6R(1-\upsilon_s)d_{AlGaN}} \tag{5}$$

where Y_{GaN}, d_{GaN}, and υ_s are the biaxial modulus,[26] thickness, and Poisson's ratio of GaN. The values of these constants used in calculations are listed in Table SI (see supplementary data, available online at stacks.iop.org/APEX/15/071011/mmedia). The AlGaN coefficient is linearly interpolated between AlN and GaN parameters for the Al concentration.

From Eq. (4b), we have a linear relationship between Q_{AlGaN} and $1/R$ with a vertical intercept $Q_{AlGaN}(0)$ corresponding to the total polarization charge under flat condition. Figure 5(c) shows both Q_{AlGaN} versus $1/R$, and the free carriers n_s versus $1/R$ for $V_{GS} = -3$ V. We choose $V_{GS} = -3$ V to minimize heating, while still being well above V_{th}. Moreover, by partially depleting the channel, we can assure that the measured triode-region resistance is dominated by the channel, and not influenced by the contacts nor access regions. As $1/R$ went from 0 (flat) to 333 m^{-1} ($R = 0.3$ cm), n_s increased by $\sim 3x$, similar to the increase in triode-region conductance. Given that the triode-region conductance is $\propto \mu_n C_{GS}(V_{GS} - V_{th}) = \mu_n n_s$, we can infer that μ_n is not strongly influenced by tensile strain in the absence of heating. This observation is in reasonable agreement with the slight

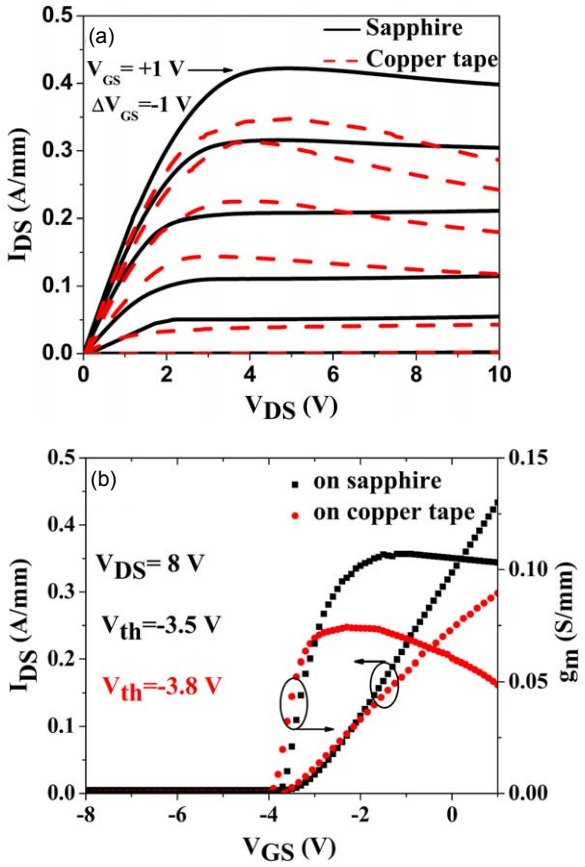

Fig. 4. (Color online) (a) Output characteristics of HEMTs on sapphire and copper tape. (b) Comparison of transfer characteristics and transconductance curves of HEMTs on sapphire and copper tape.

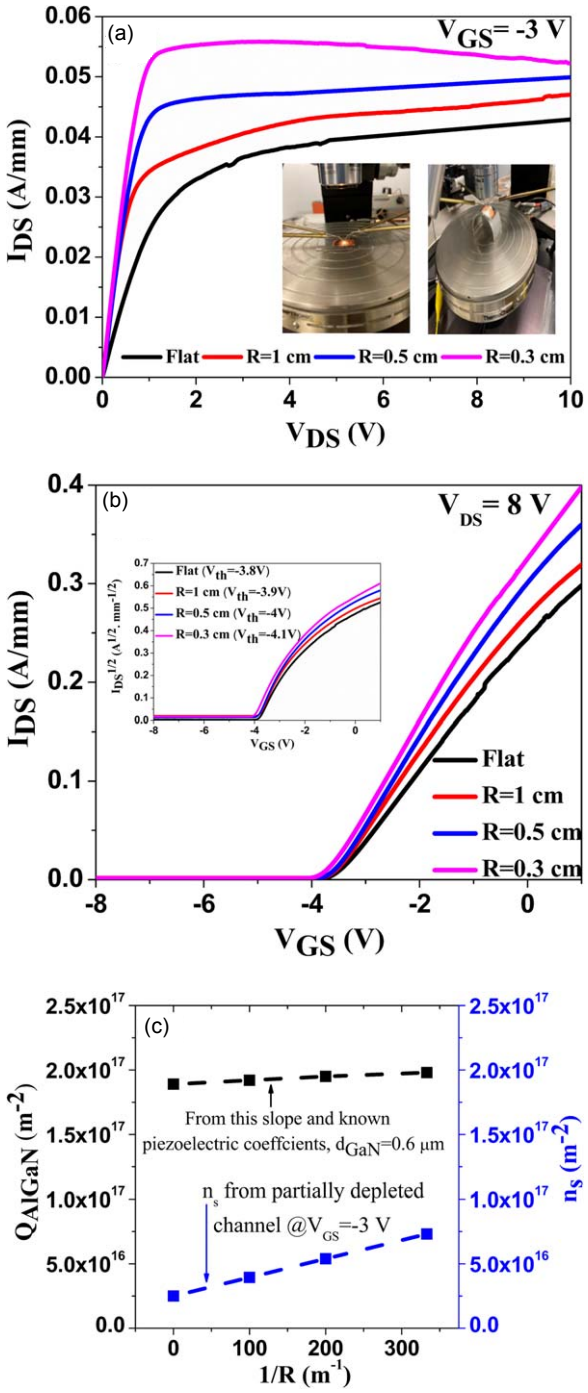

Fig. 5. (Color online) *I–V* curves under flat and bent states. (a) Output characteristics comparison showing a higher current density under bent states due to the enhanced piezoelectric polarization of AlGaN caused by tensile stress. Insets show images for the measurement setup of HEMT under flat and bent states. (b) Transfer characteristics under flat and bent states. Inset shows the change in V_{th} after bending. (c) Q_{AlGaN} and n_s as a function of $1/R$ at $V_{GS} = -3$V. The slope for n_s is sharper due to an additional shift in V_{th}.

increase observed by Azize et al[27] and the slight decrease observed by different groups,[7,10,28] although the carrier transport under strain bears further investigation.

The increase in I_{DS} under tensile strain is consistent throughout the V_{GS} range [Fig. 5(a)], as well as into saturation, although the clear thermal droop makes quantitative comparisons similar to the above discussion challenging due to reduced μ_n at higher temperatures.[29] Additional discrepancies could be due to changes in thermal management under bending as there may be improved thermal contact between the GaN and the copper through the poor thermal conductivity adhesive. Disentangling these effects is beyond the scope of this present investigation, as the influence of the adhesive is challenging to control. With proper control of the adhesion technique such as with low-temperature In-based solders, improved thermal management may be obtained, allowing the full potential performance of GaN and UWBG AlGaN to be achieved on flexible platforms.

From the slope of the line in Fig. 5(c) and the known mechanical/piezoelectric constants from Table SI (see supplementary data) in Eq. (4b), we obtain a channel layer thickness $d_{GaN} = 0.6\,\mu$m, or ∼1/3 of the starting specified thickness of 1.8 μm. This is due to the traumatic nature of LLO at the sapphire/GaN interface, with the temperature reaching above the GaN decomposition temperature 1300 K past the interface about 1 μm deep.[30] Previous studies have not accounted for this loss, and our method provides a means to measure the remaining average channel layer thickness in lifted-off flexible devices, particularly as future studies scale up to flexible UWBG AlGaN, or even AlN devices.[19]

In summary, an improved fabrication method is proposed where GaN-channel HEMTs are originally grown on sapphire substrate and transferred onto a copper tape using LLO with a drain current degradation of only ∼18%. This is lower than that reported for other transfer techniques. The effect of external stress on the 2DEG in flexible HEMT by mechanical bending is also investigated. Under tensile stress with

different radii of curvature, an increase in I_{DS} is observed. Our previous demonstration of AlN LLO from sapphire,[19] and the current study where LLO of GaN is achieved show that this LLO technique is suitable for the full AlGaN alloy system, including the UWBG AlGaN channel devices. This scalable transfer method provides the capability of large-scale, flexible III-nitride $Al_xGa_{1-x}N$ channel HEMTs for high-frequency, and high-power operation.

Acknowledgments This research was supported by the Army Research Office (ARO) (Contract No. W911NF-18-1-0029) monitored by Dr. M. Gerhold and the Office of Naval Research (ONR) Multidisciplinary University Research Initiatives (MURI) program (Contract No. N00014-18-1-2429) monitored by Mr. Lynn Petersen. The characterization was partially supported by the National Science Foundation (NSF), Electrical, Communications and Cyber Systems (ECCS) Award nos. 1711322, 1810116, and 1831954. We also acknowledge the UofSC ASPIRE program.

ORCID iDs Md Didarul Alam https://orcid.org/0000-0002-0673-6081 Shahab Mollah https://orcid.org/0000-0002-2848-2959

1) J. W. Johnson, E. L. Piner, A. Vescan, R. Therrien, P. Rajagopal, J. C. Roberts, J. D. Brown, S. Singhal, and K. J. Linthicum, IEEE Electron Device Lett. **25**, 459 (2004).
2) N. Tipirneni, A. Koudymov, V. Adivarahan, J. Yang, G. Simin, and M. A. Khan, IEEE Electron Device Lett. **27**, 716 (2006).
3) C. Lee, P. Saunier, J. Yang, and A. M. Khan, IEEE Electron Device Lett. **24**, 616 (2003).
4) J. G. Kim, C. Cho, E. Kim, J. S. Hwang, K. H. Park, and J. H. Lee, IEEE Trans. Electron Devices **68**, 1513 (2021).
5) A. Bose, D. Biswas, S. Hishiki, S. Ouchi, K. Kitahara, K. Kawamura, and A. Wakejima, IEEE Access **9**, 57046 (2021).
6) B. Duan, L. Yang, Y. Wang, and Y. Yang, IEEE Trans. Electron Devices **68**, 2240 (2021).
7) N. Defrance, F. Lecourt, Y. Douvry, M. Lesecq, V. Hoel, A. Des Lecavelier Etangs-Levallois, Y. Cordier, A. Ebongue, and J. C. De Jaeger, IEEE Trans. Electron Devices **60**, 1054 (2013).
8) M. Lesecq, V. Hoel, A. L. Des Etangs-Levallois, E. Pichonat, Y. Douvry, and J. C. De Jaeger, IEEE Electron Device Lett. **32**, 143 (2011).
9) S. Mhedhbi, M. Lesecq, P. Altuntas, N. Defrance, Y. Cordier, B. Damilano, G. Tabares Jimenéz, A. Ebongue, and V. Hoel, Phys. Status Solidi Appl. Mater. Sci. **214**, 1600484 (2017).
10) J. Zhu, X. Zhou, L. Jing, Q. Hua, W. Hu, and Z. L. Wang, ACS Nano **13**, 13161 (2019).
11) K. L. Hsu and M. C. Wu, IEEE Trans. Electron Devices **68**, 3320 (2021).
12) Y. Y. Zhang, S. An, Y. Zheng, J. Lai, J. H. Seo, K. H. Lee, and M. Kim, Adv. Electron. Mater. **8**, 2100652 (2021).
13) N. R. Glavin, K. D. Chabak, E. R. Heller, E. A. Moore, T. A. Prusnick, B. Maruyama, D. E. Walker, D. L. Dorsey, Q. Paduano, and M. Snure, Adv. Mater. **29**, 1701838 (2017).
14) X. Chen, J. Dong, C. He, L. He, Z. Chen, S. Li, K. Zhang, X. Wang, and Z. L. Wang, Nano-Micro Lett. **13**, 67 (2021).
15) T. H. Chang, K. Xiong, S. H. Park, G. Yuan, Z. Ma, and J. Han, Sci Rep. **7**, 1 (2017).
16) W. Wang, H. Wang, W. Yang, Y. Zhu, and G. Li, Sci Rep. **6**, 1 (2016).
17) H. P. Lee, J. Perozek, L. D. Rosario, and C. Bayram, Sci. Rep. **6**, 37588 (2016).
18) A. G. Baca, A. M. Armstrong, B. A. Klein, A. A. Allerman, E. A. Douglas, and R. J. Kaplar, J. Vac. Sci. Technol. A Vacuum, Surfaces, Film. **38**, 020803 (2020).
19) M. D. Alam, M. Gaevski, M. U. Jewel, S. Mollah, A. Mamun, K. Hussain, R. Floyd, G. Simin, M. V. S. Chandrashekhar, and A. Khan, Appl. Phys. Lett. **119**, 132106 (2021).
20) R. Kagawa, K. Kawamura, Y. Sakaida, S. Ouchi, H. Uratani, Y. Shimizu, Y. Ohno, Y. Nagai, N. Shigekawa, and J. Liang, 2021 7th Int. Work. Low Temp. Bond. 3D Integr. LTB-3D, 2021, p. 15, DOI: 10.1109/LTB-3D53950.2021.9598453.
21) L. Arivazhagan, A. Jarndal, and D. Nirmal, J. Comput. Electron. **20**, 873 (2021).
22) X. Hu, S. Hwang, K. Hussain, R. Floyd, S. Mollah, F. Asif, G. Simin, and A. Khan, IEEE Electron Device Lett. **39**, 1568 (2018).
23) W. Wang et al., Appl. Phys. Lett. **116**, 123501 (2020).
24) O. Ambacher et al., J. Appl. Phys. **87**, 334 (1999).
25) N. Schwarzer and F. Richter, Univ. Chemnitz, Tech. Rep. 55476433 Technische Universität Chemnitz, Chemnitz, 2006, https://nbn-resolving.org/urn:nbn:de:swb:ch1-200600111.
26) S. Choi, E. Heller, D. Dorsey, R. Vetury, and S. Graham, J. Appl. Phys. **113**, 093510 (2013).
27) M. Azize and T. Palacios, J. Appl. Phys. **108**, 023707 (2010).
28) Y. Wang, Q. Wu, S. Mao, R. Xu, B. Yan, and Y. Xu, IEEE Electron Device Lett. **42**, 677 (2021).
29) S. Arulkumaran, T. Egawa, H. Ishikawa, and T. Jimbo, Appl. Phys. Lett. **80**, 2186 (2002).
30) T. S. Kang, X. T. Wang, cf Lo, F. Ren, S. J. Pearton, O. Laboutin, Y. Cao, J. W. Johnson, and J. Kim, J. Vac. Sci. Technol. B **30**, 011203 (2012).